Supplemental Information

Skilled movements require non-apoptotic Bax/Bak pathway-mediated corticospinal circuit reorganization

Zirong Gu, Najet Serradj, Masaki Ueno, Mishi Liang, Jie Li, Mark L. Baccei, John H. Martin, and Yutaka Yoshida

Supplementary Information For this Manuscript includes the following:

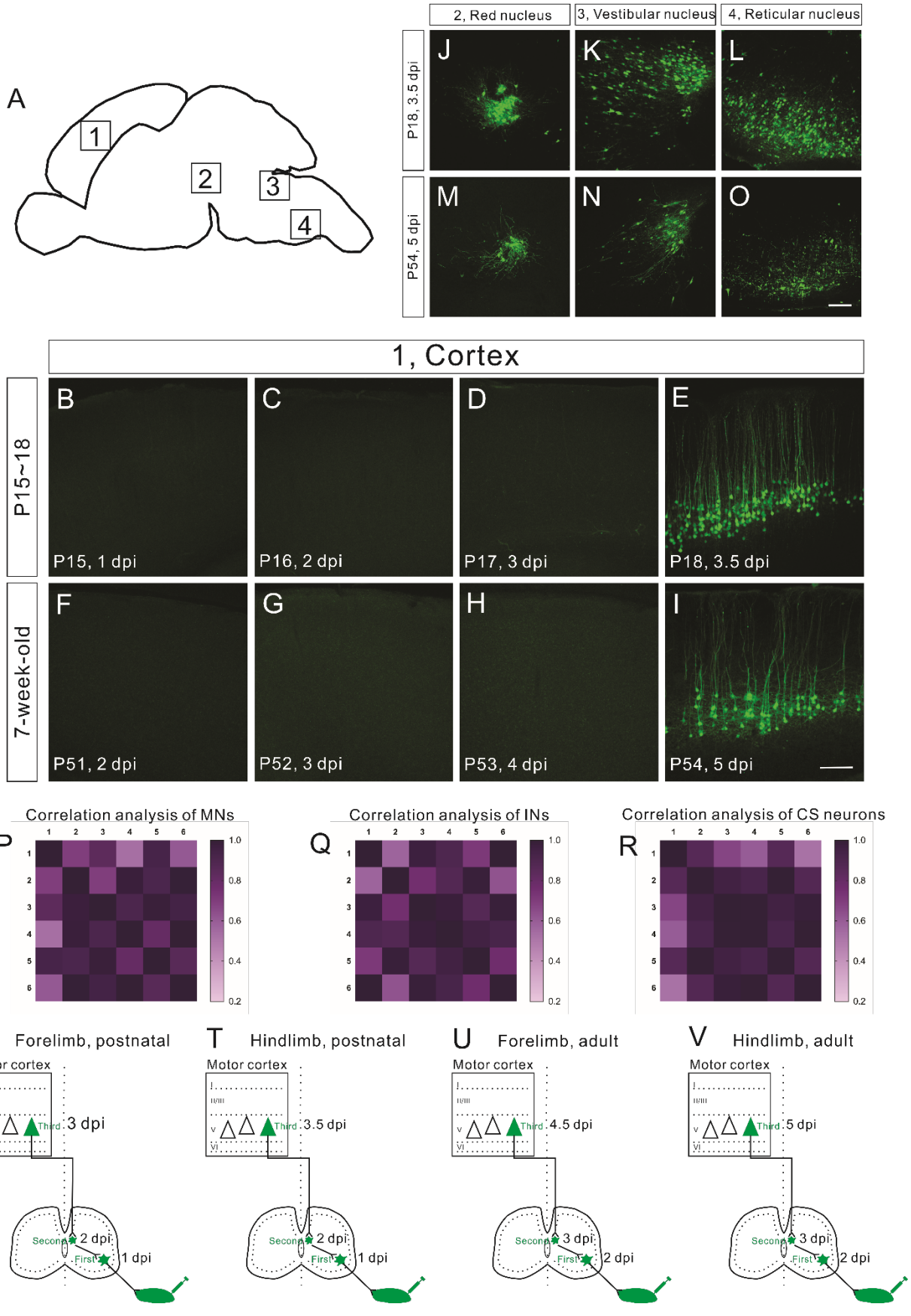
A
1
2
3
4
2, Red nucleus
3, Vestibular nucleus
4, Reticular nucleus
P18, 3.5 dpi
P54, 5 dpi
J
K
L
M
N
O
1, Cortex
P15~18
7-week-old
B
C
D
E
F
G
H
I
P15, 1 dpi
P16, 2 dpi
P17, 3 dpi
P18, 3.5 dpi
P51, 2 dpi
P52, 3 dpi
P53, 4 dpi
P54, 5 dpi
Correlation analysis of MNs
Correlation analysis of INs
Correlation analysis of CS neurons
P
Q
R
S Forelimb, postnatal
T Hindlimb, postnatal
U Forelimb, adult
V Hindlimb, adult
Motor cortex
Third
First
Second
3 dpi
3.5 dpi
4.5 dpi
5 dpi
2 dpi
1 dpi

Figure S1. Time-course of PRV tracing in descending pathways (related to Figure 1)

(A) Sagittal view of a brain section showing origins of different descending pathways: 1) the CS pathway; 2) the rubrospinal pathway; 3) the vestibulospinal pathway; and 4) the medullary reticulospinal pathway.

(B–I) Representative images of sagittal brain sections from P15~18 (B–E) and P51~54 adult (F–I) mice with PRV-eGFP injected into the Rf muscle. PRV-eGFP was only detected at 3.5 (E) and 5 (I) dpi in early postnatal and adult mice, respectively.

(J–O) Sagittal brain sections showing the labeling of the red nucleus (J and M), vestibular nucleus (K and N), and reticular nuclei (L and O) in P18 (n=8) and P54 (n=5) mice.

(P–R) Correlation analysis showing numbers of MNs, INs, and CS neurons labeled by PRV-eGFP injected into the Rf muscle at P15~18 across six different animals. Numbers of PRV-labeled neurons are highly correlated from different cases. Color scale to the right indicates correlation values.

(S–V) Summary of the PRV-tracing time course in early postnatal and adult mice (n=5~8 mice for each condition). Where "n" represents the number of mice used in each experiment. Scale bars, 200 μm (I and O).

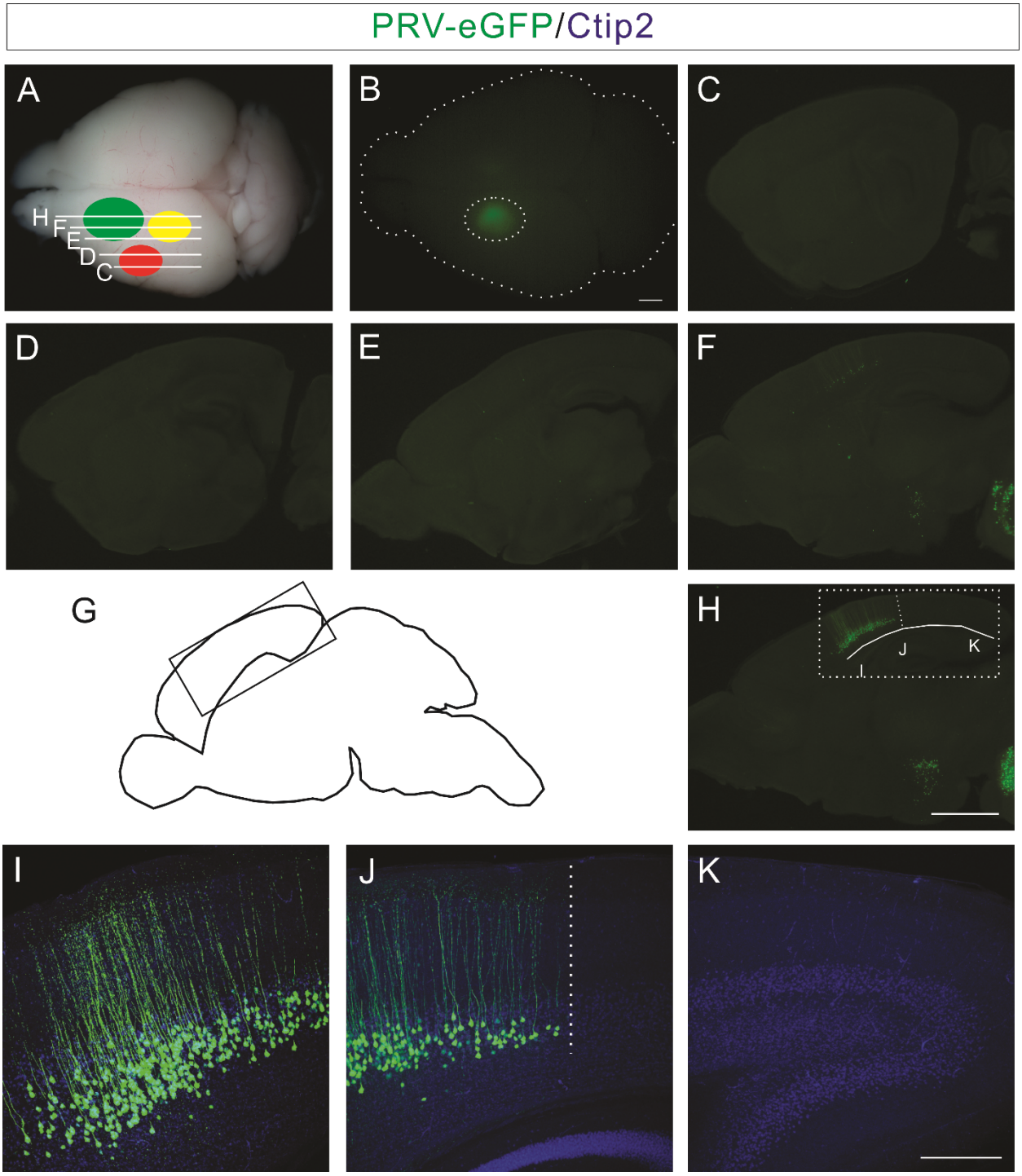
PRV-eGFP/Ctip2
A
B
C
D
E
F
G
H
I
J
K
H
F
E
D
C
J
K
I

Figure S2. CS neurons labeled by PRVs are restricted to the motor cortex (related to Figure 1)

(A–B) Representative images of a brain from mice injected with PRV-eGFP into the Rf muscle (n=8) at P18. (A) Locations of different cortical areas (motor cortex, green oval; sensory cortex, red oval; visual cortex, yellow oval). (B) Selective labeling of the motor cortex by PRV-eGFP (dotted oval).

(C–F and H) Representative sagittal brain sections showing neurons labeled by PRV-eGFP. Most PRV-eGFP$^+$ CS neurons are located at the center of the motor cortex (white dotted rectangle in H). Note the absence of PRV-eGFP$^+$ neurons in the sensory cortex (C–E).

(G) Schematic of sagittal brain section, illustrating the location of the motor cortex and the adjacent cortical areas (black rectangle).

(I–K) Magnified views of boxed area in (H) showing the restriction of PRV-eGFP labeled CS neurons to the motor cortex (note: PRV-eGFP$^+$ CS neurons also express Ctip2 (blue)). PRV-eGFP is restricted to the motor cortex (I and J) and is absent from the visual cortex (K) (the border between the motor and visual cortices is indicated by the white dotted line in J). Where "n" represents the number of mice used in each experiment. Scale bars, 200 μm (K), 500 μm (H) and 1 mm (B).

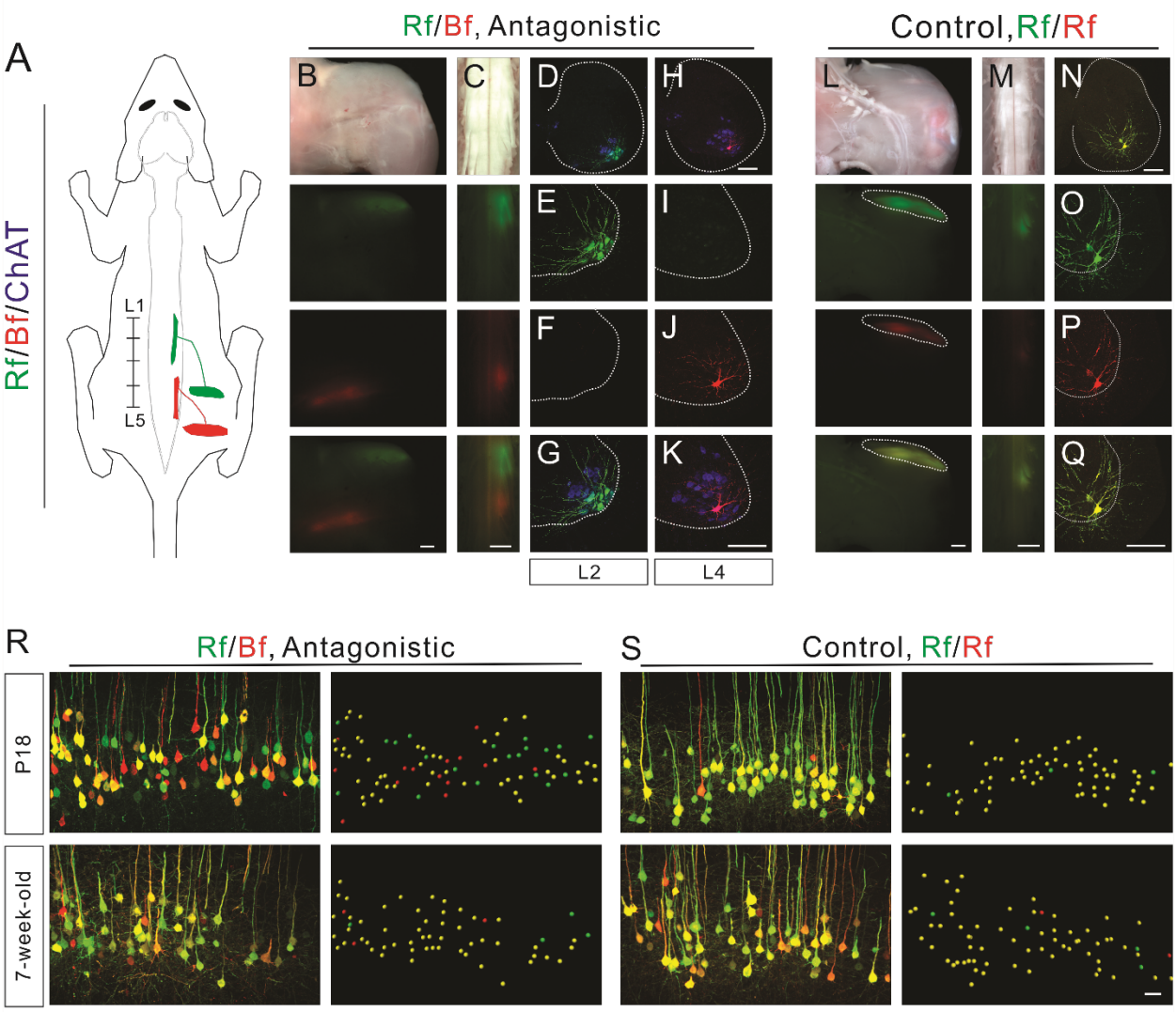

Figure S3. A dual-color PRV tracing experiment from a pair of antagonistic hindlimb muscles (related to Figures 1 and 2)

(A) Diagram illustrating motor neuron pools labeled by retrograde tracing from a pair of antagonistic muscles in the hindlimb, Rf (PRV-eGFP) and Bf (PRV-RFP).

(B and C) Color (top one) and fluorescent (bottom three) images of hindlimb muscles (B) and spinal cords (C) at 2 dpi (n=5).

(D–K) Transverse spinal cord sections showing the labeling of PRV-eGFP$^+$ Rf and PRV-RFP$^+$ Bf motor neurons in ChAT$^+$ (blue) motor neuron pools at lumbar levels 2 (D–G) and 4 (H–K) at 1 dpi, respectively. When we injected two color variants of PRVs to different muscles including (Rf/Bf), we never observed double labeled-cells in muscles and MNs (data not shown), indicating that injected PRVs are restricted to a specific muscle.

(L–M) Color (top one) and fluorescent (bottom three) images of hindlimb muscles (L) and spinal cords (M) at 2 dpi (n=6) from a control experiment in which a mixture of PRV-eGFP and PRV-RFP was injected into the Rf muscle at P14. Note the viruses were restricted to the target muscle (indicated by the white dashed circles in figures under L).

(N–Q) Transverse lumbar spinal cord sections showing labeling of PRV-eGFP$^+$ and PRV-RFP$^+$ Rf motor neurons at 1 dpi (n=5).

(R) Representative images of CS neurons labeled by dual-color PRV tracing from the Rf/Bf muscle pair at early postnatal (top, n=6) and adult (bottom, n=6) stages.

(S) Representative images of CS neurons labeled by injections of the PRV-eGPF and PRV-RFP mixture into the Rf muscle at postnatal (top, n=3) and adult (bottom, n=6) stages. Where "n" represents the number of mice used in each experiment. Scale bars, 50 μm (S), 200 μm (K and Q), and 1 mm (B, C, L, and M).

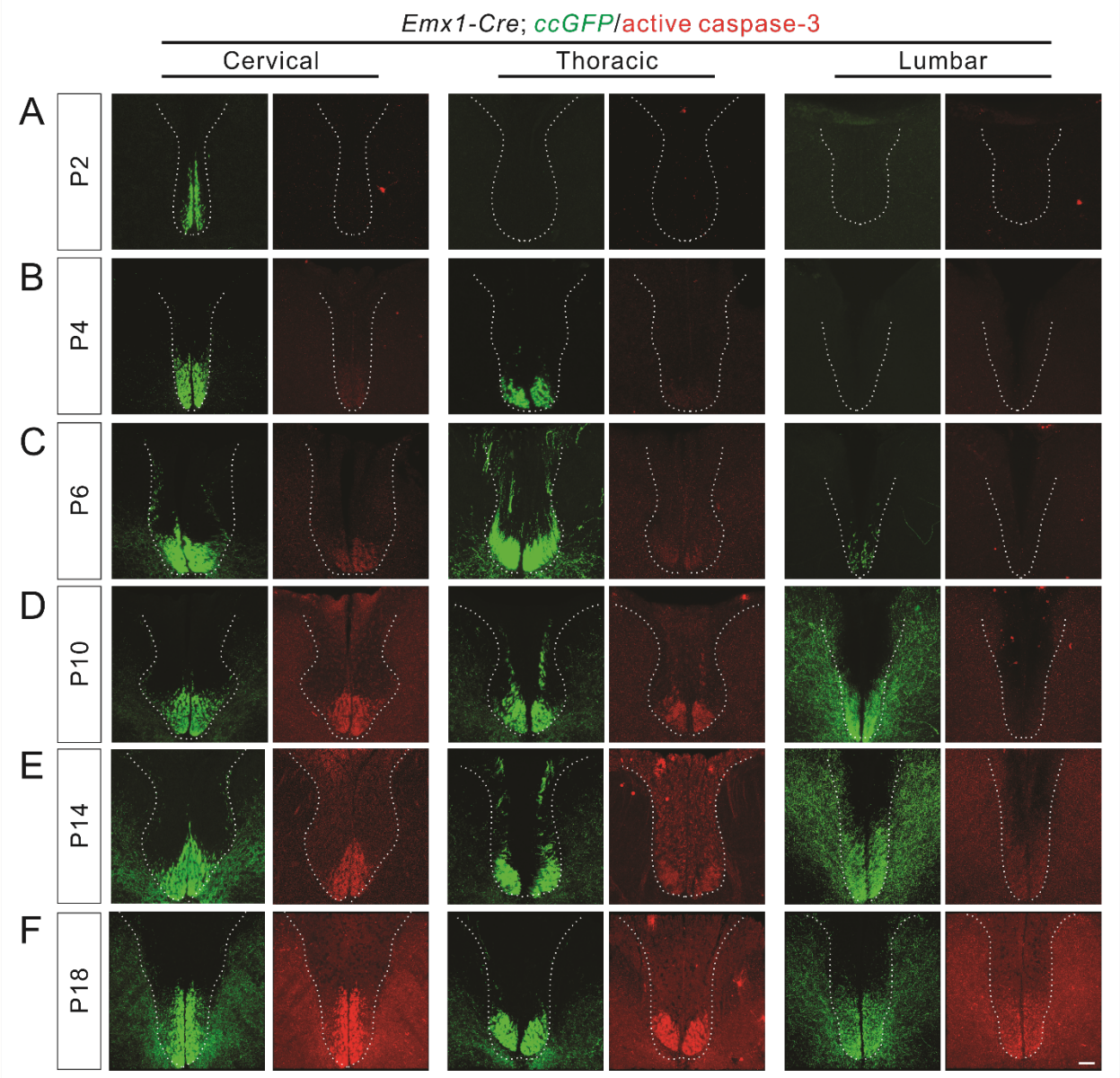

Figure S4. Activation of caspase-3 in descending CS axons during CS circuit development (related to Figure 4)

(A–F) Expression of active caspase-3 (red) in CS axons (green) within the dorsal funiculus (indicated by white dashed lines) of cervical, thoracic, and lumbar spinal cords from P2 (A), P4 (B), P6 (C), P10 (D), P14 (E), and P18 (F) *Emx1-Cre*; *ccGFP* mice (n=3 mice for each stage). Scale bar, 50 μm (F).

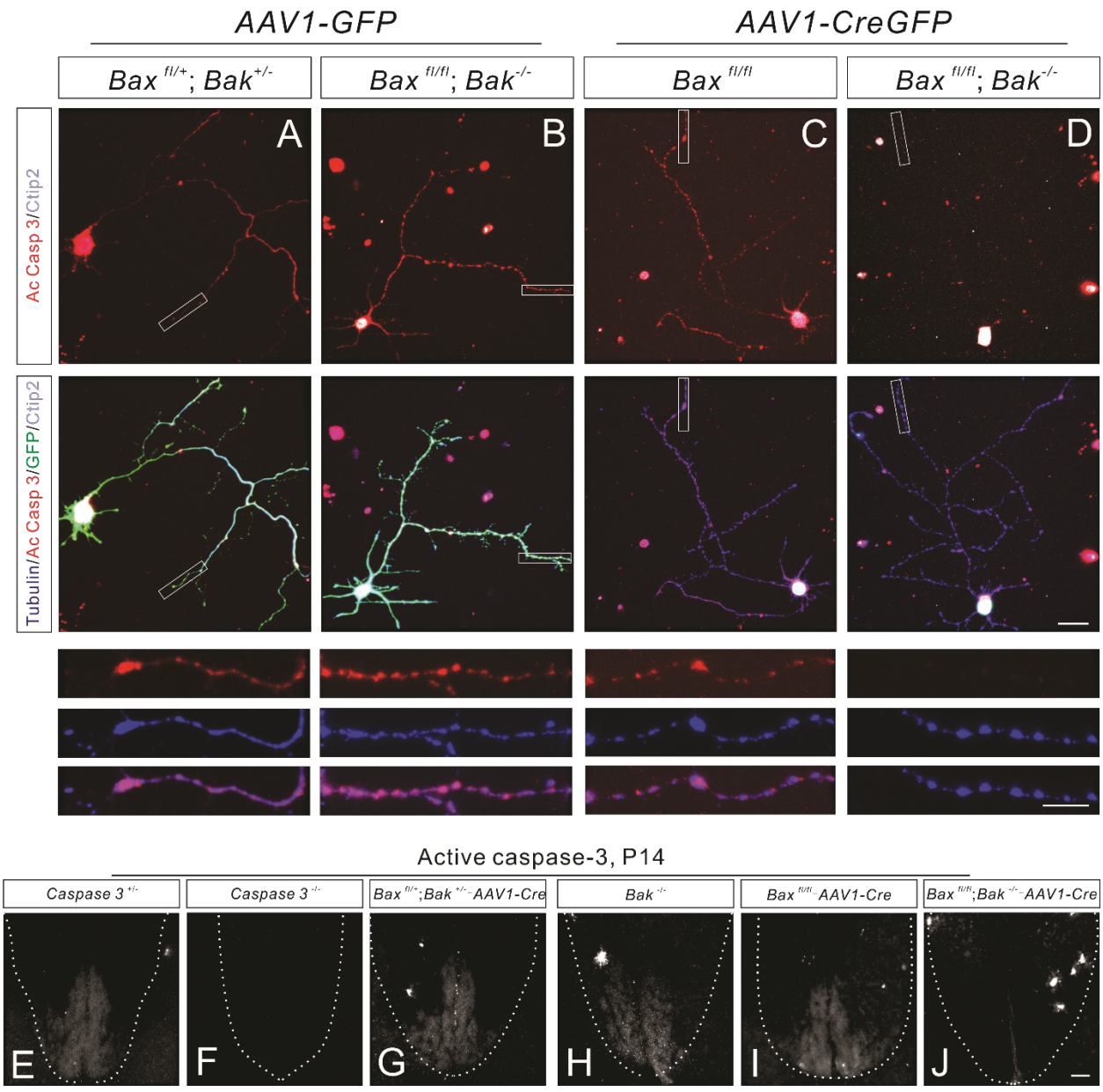
AAV1-GFP
AAV1-CreGFP
Bax fl/+; Bak +/-
Bax fl/fl; Bak -/-
Bax fl/fl
Bax fl/fl; Bak -/-
A
B
C
D
Ac Casp 3/Ctip2
Tubulin/Ac Casp 3/GFP/Ctip2
Active caspase-3, P14
Caspase 3 +/-
Caspase 3 -/-
Bax fl/+;Bak +/--AAV1-Cre
Bak -/-
Bax fl/fl-AAV1-Cre
Bax fl/fl;Bak -/--AAV1-Cre
E
F
G
H
I
J

Figure S5. Axonal localized activation of caspase-3 requires Bax and Bak (related to Figure 4)

(A–D) Immunostaining of cultured cortical neurons (7 days *in vitro*) from *Bax*$^{fl/fl}$, *Bax*$^{fl/+}$; *Bak*$^{+/-}$, and *Bax*$^{fl/fl}$; *Bak*$^{-/-}$ mice showing GFP (green), active caspase-3 (red), Tubulin (blue), and Ctip2 (gray). *AAV1-CreGFP* was used to deliver Cre recombinase, and *AAV1-GFP* was used as a control. Note, CreGFP is a fusion protein and is restricted to the nucleus.

(E–J) Expression of active caspase-3 in the dorsal funiculus (indicated by white dashed lines) of cervical spinal cords from P14 *caspase-3*$^{+/-}$ (E), *caspase-3*$^{-/-}$ (F), *Bax*$^{fl/+}$; *Bak*$^{+/-}$*-AAV1-Cre* (G), *Bak*$^{-/-}$ (H), *Bax*$^{fl/fl}$*-AAV1-Cre* (I), and *Bax*$^{fl/fl}$; *Bak*$^{-/-}$*-AAV1-Cre* (J) mice (n=3 mice for each genotype). Scale bars, 20 μm (magnified view of D), and 50 μm (D and J).

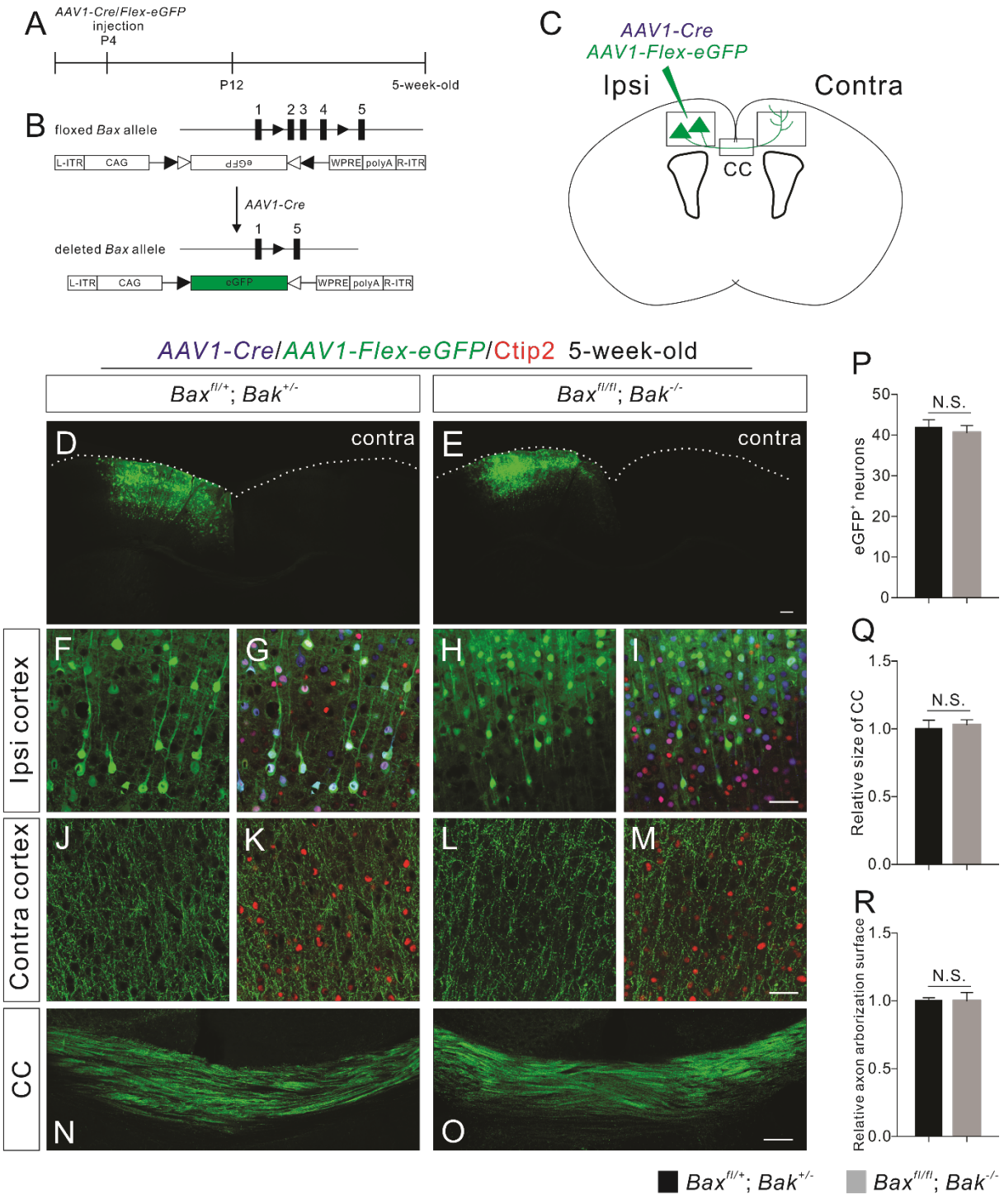
A
AAV1-Cre/Flex-eGFP
injection
P4
P12
5-week-old
B
floxed Bax allele
1 2 3 4 5
L-ITR CAG eGFP WPRE polyA R-ITR
AAV1-Cre
deleted Bax allele
1 5
L-ITR CAG cGFP WPRE polyA R-ITR
C
AAV1-Cre
AAV1-Flex-eGFP
Ipsi
Contra
CC
AAV1-Cre/AAV1-Flex-eGFP/Ctip2 5-week-old
Bax^fl/+; Bak^+/-
Bax^fl/fl; Bak^-/-
D
contra
E
contra
Ipsi cortex
Contra cortex
CC
F
G
H
I
J
K
L
M
N
O
P
eGFP+ neurons
N.S.
Q
Relative size of CC
N.S.
R
Relative axon arborization surface
N.S.
Bax^fl/+; Bak^+/-
Bax^fl/fl; Bak^-/-

Figure S6. No obvious defects in cortico-cortical axonal tracts in *Bax$^{fl/fl}$*; *Bak$^{-/-}$-AAV1-Cre* mice (related to Figure 4)

(A) Experimental design. A mixed virus solution (*AAV1-Cre* and a Cre-dependent eGFP reporter AAV virus) was injected into the motor cortex to delete the floxed *Bax* allele and label CS axons in P4 mice. Brains and spinal cords were analyzed at P12 and 5-week-old stages.

(B) Strategy for conditional deletion of the floxed *Bax* allele in the motor cortex to create *Bax$^{fl/fl}$*; *Bak$^{-/-}$-AAV1-Cre* mice. Schematic representation of the loxP sequences flanking exons 2–4 of the *Bax* gene. Exons 2–4 are deleted after *AAV1-Cre* mediated recombination. A Cre-dependent eGFP reporter AAV virus is used to label axons of Bax/Bak-deficient CS neurons in *Bax$^{fl/fl}$*; *Bak$^{-/-}$-AAV1-Cre* mice.

(C) Schematic of a coronal section of the brain showing the corpus callosum (CC) fibers and axonal arbors in the contralateral side of the cortex labeled by the AAV virus.

(D–O) Coronal brain sections from 5-week-old mice were immunostained for eGFP (green), Ctip2 (red), and Cre (blue), showing low magnification images (D and E) and high magnification images (F–O) of boxed areas in C.

(F–I) Ipsilateral side of the cortex from *Bax$^{fl/+}$*; *Bak$^{+/-}$-AAV1-Cre* (control) (F and G) and *Bax$^{fl/fl}$*; *Bak$^{-/-}$-AAV1-Cre* (H and I) mice showing GFP^{+} CS neurons.

(J–M) Contralateral side of the cortex from control (J and K) and *Bax$^{fl/fl}$*; *Bak$^{-/-}$-AAV1-Cre* (L and M) mice showing eGFP^{+} axonal arbors from the ipsilateral side of the cortex.

(N and O) High magnification view of the CC from the middle boxed area in (C) showing CC fibers from control (N) and *Bax$^{fl/fl}$*; *Bak$^{-/-}$-AAV1-Cre* (O) mice.

(P) Quantification of $eGFP^+$ CS neurons showing that similar numbers (P=0.6637) of $eGFP^+$ neurons were labeled by viruses in control (*Bax*$^{fl/+}$; *Bak*$^{+/-}$*-AAV1-Cre*, n=8) and *Bax*$^{fl/fl}$; *Bak*$^{-/-}$*-AAV1-Cre* mice (n=8).

(Q) Relative sizes of CC fibers. CC fibers labeled by AAV viruses were similar (P=0.7349) in size between control (n=8) and *Bax*$^{fl/fl}$; *Bak*$^{-/-}$*-AAV1-Cre* mice (n=8).

(R) $eGFP^+$ axon arborization surface areas in the contralateral side of the cortex labeled by AAV viruses were similar between control (n=8) and *Bax*$^{fl/fl}$; *Bak*$^{-/-}$*-AAV1-Cre* mice (P=0.9505, n=8). Where "n" represents the number of mice used in each experiment. Scale bars, 50 μm (I and M), 100 μm (O), and 500 μm (E).

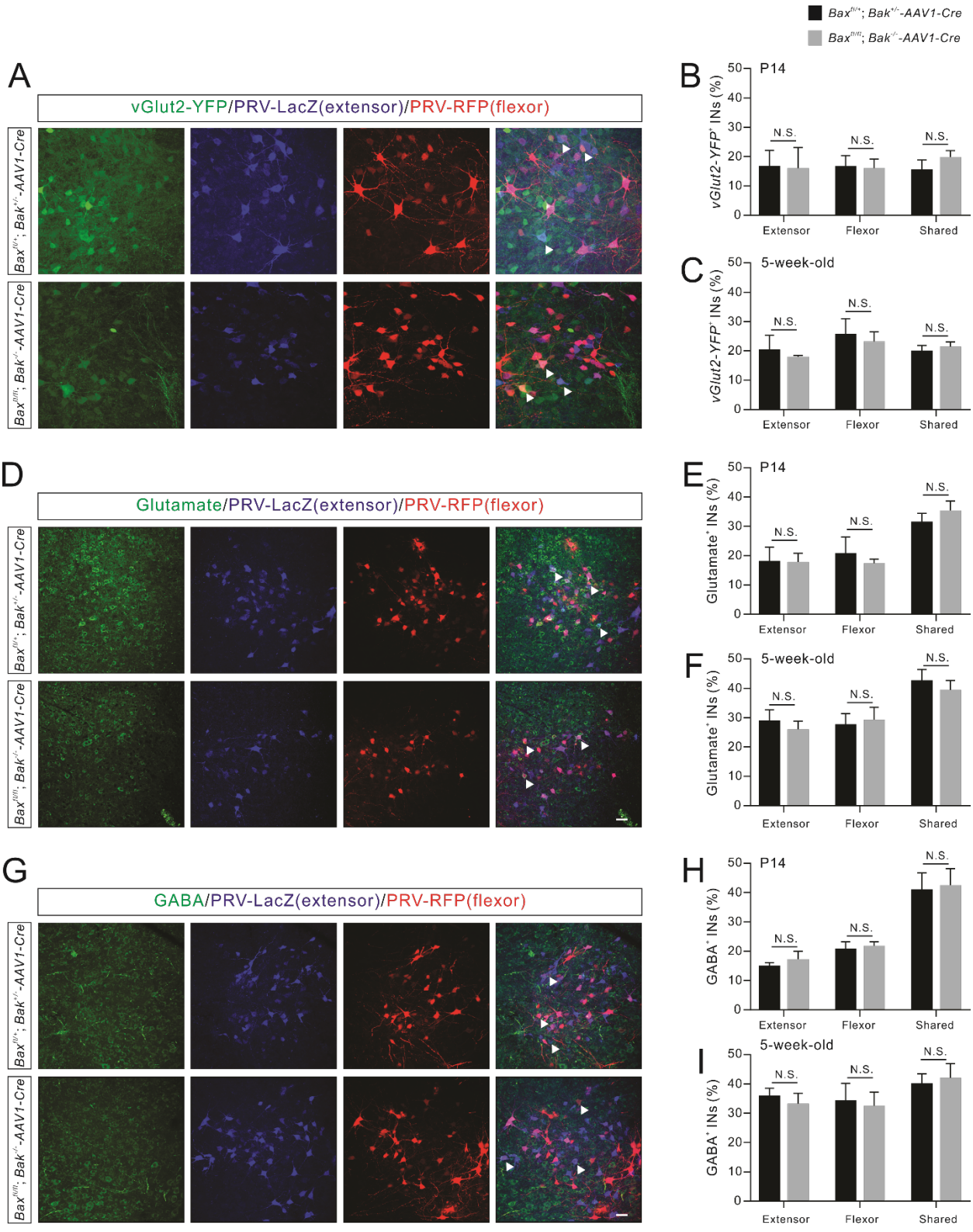
A
vGlut2-YFP/PRV-LacZ(extensor)/PRV-RFP(flexor)
Bax+/+; Bak+/--AAV1-Cre
Bax f/f; Bak-/--AAV1-Cre
B
P14
vGlut2-YFP+ INs (%)
N.S.
Extensor
Flexor
Shared
C
5-week-old
D
Glutamate/PRV-LacZ(extensor)/PRV-RFP(flexor)
E
Glutamate+ INs (%)
F
G
GABA/PRV-LacZ(extensor)/PRV-RFP(flexor)
H
GABA+ INs (%)
I

Figure S7. No obvious defects in IN-MN connectivity in *Bax$^{fl/fl}$*; *Bak$^{-/-}$-AAV1-Cre* (related to Figure 6)

(A) Cervical spinal cord sections from P14 *Bax$^{fl/+}$*; *Bak$^{+/-}$-AAV1-Cre* (control, top panels) and *Bax$^{fl/fl}$*; *Bak$^{-/-}$-AAV1-Cre* mice (bottom panels) mice were immunostained for eGFP (green for *vGlut2-YFP*), LacZ (blue), and RFP (red), showing that subsets of PRV-infected INs are *vGlut2-YFP* positive (representative INs indicated by white arrowheads).

(B and C) Similar fractions of INs (extensor, P=0.9334 at P14, P=0.6176 at adult; flexor, P=0.8972 at P14, P=0.7129 at adult; shared P=0.3524 at P14, P=0.6525 at adult) are *vGlut2-YFP^{+}* in P14 (B) and 5-week-old adult (C) control (P14, n=8; adult, n=7) and *Bax$^{fl/fl}$*; *Bak$^{-/-}$-AAV1-Cre* mice (P14, n=7; adult, n=8) .

(D) Cervical spinal cord sections from P14 control (top panels) and *Bax$^{fl/fl}$*; *Bak$^{-/-}$-AAV1-Cre* mice (bottom panels) mice were immunostained for glutamate (green), LacZ (blue), and RFP (red). Subsets of PRV-infected INs are glutamate positive (representative INs indicated by white arrowheads).

(E and F) Similar fractions of INs are glutamate positive (extensor, P=0.9507 at P14, P=0.5557 at adult; flexor, P=0.5493 at P14, P=0.8160 at adult; shared P=0.4460 at P14, P=0.5497 at adult) in P14 (E) and adult (F) control (P14, n=7; adult, n=6) and *Bax$^{fl/fl}$*; *Bak$^{-/-}$-AAV1-Cre* mice (P14, n=8; adult, n=7).

(G) Cervical spinal cord sections from P14 control (top panels) and *Bax$^{fl/fl}$*; *Bak$^{-/-}$-AAV1-Cre* mice (bottom panels) mice were immunostained for GABA (green), LacZ (blue), and RFP (red), showing subsets of PRV-infected INs are GABA positive (representative INs indicated by white arrowheads).

(H and I) Similar fractions of INs (extensor, P=0.5730 at P14, P=0.5627 at adult; flexor, P=0.7545 at P14, P=0.8174 at adult; shared P=0.8638 at P14, P=0.7817 at adult) are GABA positive in P14 (E) and adult (F) control (P14, n=6; adult, n=9) and $Bax^{fl/fl}$; $Bak^{-/-}$-*AAV1-Cre* mice (P14, n=8; adult, n=8). Where "n" represents the number of mice used in each experiment. Scale bars, 50 μm.

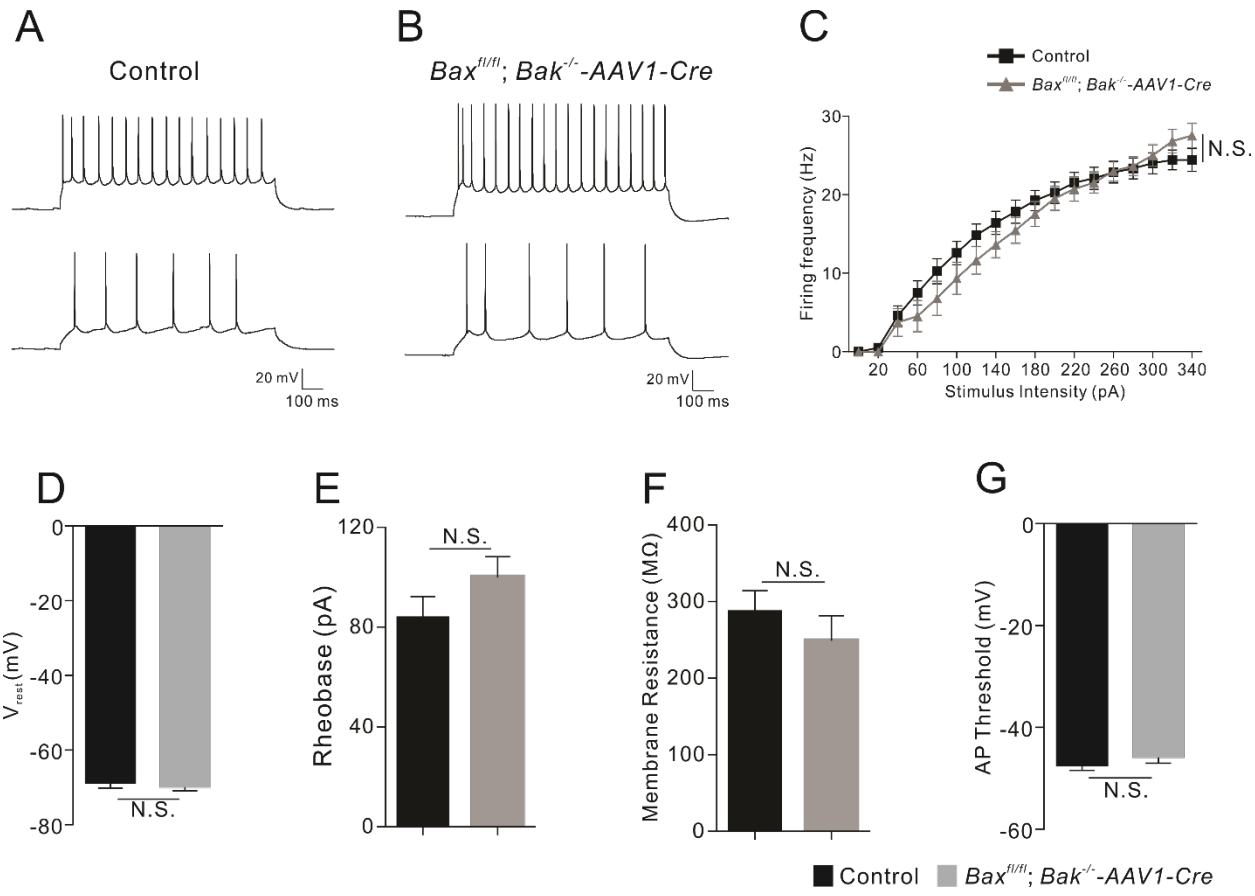
A
Control
20 mV
100 ms
B
Bax^fl/fl; Bak^-/--AAV1-Cre
20 mV
100 ms
C
Control
Bax^fl/fl; Bak^-/--AAV1-Cre
Firing frequency (Hz)
Stimulus Intensity (pA)
N.S.
D
V_rest (mV)
N.S.
E
Rheobase (pA)
N.S.
F
Membrane Resistance (MΩ)
N.S.
G
AP Threshold (mV)
N.S.
Control
Bax^fl/fl; Bak^-/--AAV1-Cre

Figure S8. Normal neuronal excitability in *Bax*/*Bak*-deficient CS neurons (related to Figure 7)

(A and B) Examples of action potential discharges evoked in CS neurons in brain slices prepared from control (wild-type mice receiving *AAV1-Cre* injections at P2) (A) and $Bax^{fl/fl}$; $Bak^{-/-}$-*AAV1-Cre* (B) mice during intracellular current injections (100 pA, bottom; 220 pA, top) through the patch clamp electrode.

(C) The two groups exhibited similar ($P>0.05$) firing frequencies across a range of stimulus intensities *in vitro*.

(D–E) There were no significant effects of *Bax/Bak* deletion on the resting membrane potential (D, n=12 neurons in each group; P=0.5237) or rheobase (E, P=0.1849) in CS neurons.

(F) There were no significant differences in membrane resistances in CS neurons between control and $Bax^{fl/fl}$; $Bak^{-/-}$-*AAV1-Cre* mice (n=12 neurons in each group; P=0.3839).

(G) Action potential thresholds were also similar (P=0.2824) between the two experimental groups.

Supplemental Movie S1. Representative movie showing the performance of an adult *Bax*$^{fl/+}$; *Bak*$^{+/-}$*-AAV1-Cre* mouse on the reaching test (related to Figure 8).

Representative movie showing the performance of an adult *Bax*$^{fl/+}$; *Bak*$^{+/-}$*-AAV1-Cre* (*AAV1-Cre* injection was performed at P2) mouse on the reaching test.

Supplemental Movie S2. Representative movie showing the performance of an adult *Bax*$^{fl/fl}$; *Bak*$^{-/-}$*-AAV1-Cre* mouse on the reaching test (related to Figure 8).

Representative movie showing the performance of an adult *Bax*$^{fl/fl}$; *Bak*$^{-/-}$*-AAV1-Cre* mouse (*AAV1-Cre* injection was performed at P2) on the reaching test.